Focused Ultrasound Assisted Delivery of Thiolated Nanoparticles in Tumor Microenvironments

Jackson Tirrell[a]. Krishan Perumal[a], Anna Debski[a], Richard Price, Ph.D[a,1]

[a] University of Virginia Department of Biomedical Engineering

[1] Correspondence: rjp2z@virginia.edu

Number of words: 4356
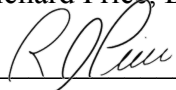
Number of figures and tables: 11

Number of equations: 0

Number of supplements: 4

Number of references: 36

ADVISORS

Dr. Richard Price, Department of Biomedical Engineering

Signature: _____ Date: 5/6/2024

Focused Ultrasound Assisted Delivery of Thiolated Nanoparticles in Tumor Microenvironments

Jackson Tirrell[a]. Krishan Perumal[a], Anna Debski[a], Richard Price, Ph.D[a,1]

[a] University of Virginia Department of Biomedical Engineering
[1] Correspondence: rjp2z@virginia.edu

Abstract

Brain cancers such as glioblastomas are the most common central nervous system tumors and are extremely aggressive with rapid development and poor clinical outlooks [1]. The endothelial cells form the Blood Brain Barrier (BBB) and act as a barrier and a mediator between the blood and the brain through the formation of tight junctions [2]. The BBB can be bypassed by combining focused ultrasound (FUS) therapy with a microbubble injection which causes temporary tight junction opening [3]. To take advantage of the increased free thiols of tumor microenvironments (TME), we have developed a thiolated nanoparticle that leverages the free thiols of the TME as a means to target and deliver therapeutics specifically to cancerous cells. We have validated the presence of increased thiols in cancer cell lines. Additionally, we have generated a thiolated nanoparticle that shows an increased transfection efficiency to binding efficiency ratio compared to unthiolated controls. We have designed a protocol to alter the number of these thiol groups to determine the most ideal concentration. We then used this nanoparticle in conjunction with FUS to show that together these two therapeutic techniques together show more efficient transfection in a multitude of cell lines than without FUS. These findings show promise for the future implications of these thiolated nanoparticles as an effective aided delivery tool for targeted glioblastoma therapy.

Keywords: Glioblastoma, Nanoparticles, Focused Ultrasound

Introduction

Brain Cancer:

Brain cancers such as glioblastomas are the most common central nervous system tumors and are extremely aggressive with rapid development and suboptimal response to immunotherapy [1], [4], [5]. Glioblastomas, a subgroup of gliomas (primary brain tumors), are characterized partly by low levels of leukocytes and are thus considered cold tumors [6], [7]. Glioblastomas are astrocytic tumors and thus develop from astrocytes which are specialized glial cells that help stabilize and regulate the blood-brain barrier [8]. Symptoms of brain tumors include mental impairment, seizures, and headaches, all of which can have a traumatic impact on one's life [1], [9]. For children, brain cancer is the second leading cause of cancer mortality; for those under 34, it is fourth [9]. Currently, patients have a mean survival of approximately 15 months after diagnosis, and procedures intending to treat these tumors have low success rates [9]. This difficulty in treatment is in part because multiple lesions sometimes occur along with infiltrative growth and local metastasis thus making complete surgical excision near impossible [10], [11]. Current treatment options cost patients on average $106,896 over 6 months and around $25 billion is spent each year on cancer research [12], [13]. New innovative techniques are needed to help those with brain tumors, such as glioblastomas, survive and recover because the current techniques are not effective enough, evidenced by the poor outlook. Additionally, the development and implementation of effective treatments could significantly lower the financial burden on both patients and taxpayers.

Blood-Brain Barrier:

Microvascular endothelial cells are the main type of cell found in the blood-brain barrier (BBB), with pericytes and astrocytes surrounding them (Figure 1) [2]. The endothelial cells act as a barrier and a mediator
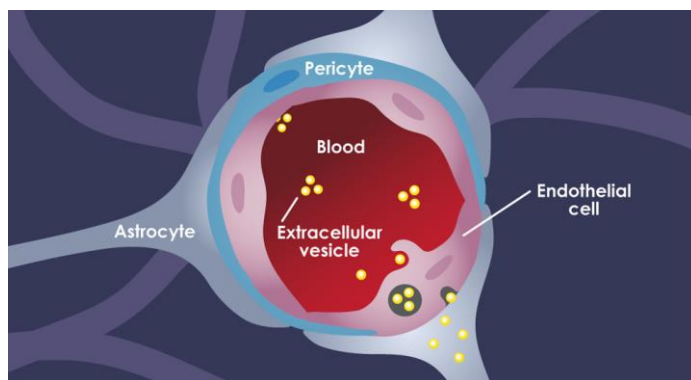

Figure 1: Diagram of the BBB illustrating interactions between blood vessels, endothelial cells, astrocytes, and pericytes.

between the blood and the brain [2], [14]. Endothelial cells of the brain form tight junctions limiting what can enter the brain from the bloodstream, and these cells repulse charged compounds [5]. The BBB protects the brain from toxic substances and can limit the movement of inflammatory cells into the brain parenchyma [2]. The tight junctions of the BBB can maintain homeostasis due to this highly selective barrier but this barrier also has negative effects such as the blocking ~100% of large-molecule neurotherapeutics and more than 98% of all small-molecule drugs [14], [16]. This effect causes difficulties in delivering any therapy to the brain. The BBB can be bypassed by combining focused ultrasound therapy with microbubble injection [3]. This therapeutic method temporarily opens specific areas of the BBB, allowing more effective drug delivery but even with this increased effectiveness the delivery is not as effective as delivery to other tissues [3]. Effective drug delivery

past the BBB remains a prominent challenge to be solved and additional techniques to optimize delivery past this barrier are needed.

Tumor Microenvironment:
The tumor microenvironment (TME), is a complex and dynamic environment that plays a crucial role in the growth, progression, and response to therapy of solid tumors [17]. It encompasses a vast array of cellular and non-cellular components that interact within and around the tumor mass [17], [18]. The TME consists of various cell types, including cancer cells, immune cells, fibroblasts, and endothelial cells [17], [19]. Each of these cell types has distinct roles within the microenvironment such as the immune cells either inhibiting or promoting tumor growth, depending on their state [20]. The TME is also home to new blood vessels formed via angiogenesis, these vessels tend to be leaky which can lead to hypoxic conditions [18]. These changes to the vasculature contribute to the weakening of the BBB and as such it is sometimes referred to as the Brain Tumor Barrier (BTB) instead [21]. In the TME, there is an increase in the concentration of free thiols. GSH is a tripeptide molecule consisting of cysteine, glutamic acid, and glycine, and it plays a crucial role in maintaining the redox balance within cells [22], [23], [24]. In cancer cells, this balance is often disrupted, thus leading to an elevated concentration of GSH [24], [25]. This elevated free thiol level due to increased GSH offers a potential therapeutic target that will be exploited by this project.
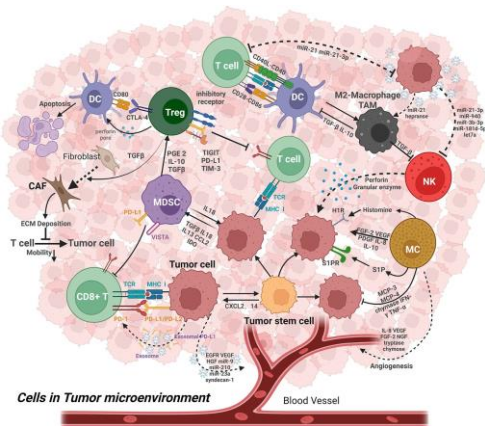

Figure 2: Diagram of complex interactions present in the TME.

Current Delivery Methods:
Many different delivery methods exist for cancer treatments. Liposomes are the most commonly used nanocarriers and are composed of lipid bilayers that closely resemble the structure of cell membranes [26]. Liposomes are considered biocompatible and encapsulate both hydrophobic and hydrophilic therapeutic agents effectively [27]. The nanoparticle being explored in this project is a polymeric nanoparticle. General polymeric nanoparticles are more stable than liposomes and have preparation methods that are easier to produce, additionally, drugs can be
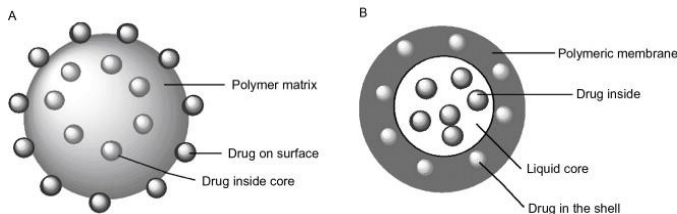

Figure 3: Polymer nanoparticle diagram illustrating their ability to hold drug doses on inside and/or outside.

placed inside or attached to the outside of these nanoparticles (Figure 2) [27], [28]. Additionally, these nanoparticles can be engineered to release drugs in a controlled manner and can be surface-modified for targeting easier than liposomes [26], [27], [29]. This surface modification property is what allows for thiolation in the nanoparticle in this project.

Hypothesis, Aims, and Constraints

This project aimed to provide foundational research that will lead to a future cancer therapy that improves the outlook for patients. This goal is challenged by many difficulties such as the properties of the BBB and the lack of current effective therapy options. As stated above, it has been found that TMEs show an increased level of exofacial thiols relative to benign cells [29]. To take advantage of this unique property of TMEs, **we proposed to develop a thiolated nanoparticle design that leverages the increased levels of free thiols in TMEs as a means to target and deliver therapeutics specifically to cancerous cells.** The following specific aims served to categorize this project's phases and illustrate a framework for the project's progression.

Aim 1: Interrogate exofacial thiol levels on multiple different cell lines
    A. Generate a protocol for the utilization of Ellman's reagent in mouse brain endothelial cells (bEnd.3) and murine glioma cells (GL261) (both *in vitro*) to color free-thiol groups for colorimetric quantification.
    B. Measure and compare the free thiol levels in the two aforementioned cell cultures using a spectrophotometer at 412 nm to confirm if the cancerous GL2621 cell line has greater numbers of thiols than the bEnd.3 cell line. Thus confirming whether the free thiols are a robust target for nanoparticles in the chosen brain model.

Aim 2: Design, synthesize, and test thiolated nanoparticles to gauge specific drug delivery efficacy
    A. Effectively synthesize thiolated and non-thiolated nanoparticles (+/- 2 mV zeta potential & 40-60 nm diameter, quantified using dynamic light scattering from Zetasizer).
    B. To gauge efficacy, measure the nanoparticle binding efficiency via a fluorescent tag and compare it to the non-thiolated nanoparticle control.
    C. Based on the assay results, optimize the number of thiol groups on the nanoparticle's surface, size, and main body composition by changing the parameters of the synthesis protocol.

Aim 3: Utilize FUS and microbubbles for nanoparticle binding to the TME
    A. Optimize FUS protocol with microbubbles and nanoparticle injection for the enhanced permeation of the thiolated nanoparticles through the BBB in a mouse model.
    B. Measure FUS optimization and plasmid delivery efficacy with a GFP fluorophore plasmid in the nanoparticles, allowing for flow cytometry analysis.

Working to accomplish these specific aims augmented our understanding and capability to innovatively and effectively address the challenges posed by glioblastomas and similar brain cancers. Our approach aimed to enhance the precision and efficiency of drug delivery directly to the tumor site, minimizing systemic exposure and potential side effects, while also circumventing the challenges presented by the BBB. The synergy of these innovations could potentially greatly extend the median survival rate of patients and have greater outcomes than current treatments, improving the quality of life for those afflicted with these devastating diseases.

Design Constraints

This project revolved around the completion of the specific aims: Comparing exofacial thiol levels between GL261 cells and bEnd.3 cells (Specific Aim I), synthesizing and testing the nanoparticles for binding and transfection efficiency (Specific Aim II), and utilizing FUS to enable the delivery of these nanoparticles *in vivo* (Specific Aim III). We adhered to specific design constraints and metrics to ensure our project's success. These served as benchmarks for evaluating the performance and viability of our nanoparticles throughout the development process. The following table (Table 1) presents a clear outline of our target parameters for the nanoparticle design.

Need #	Design Constraint/Metric	Unit of Measurements	Ideal	Marginal
1	Binding Efficiency	% Fluorescence (Cy5 labeled)	60%	30%
2	Transfection Efficiency	% Fluorescence (GFP reporter plasmid)	40%	20%
3	Zeta Potential*	mV	+2 mV	0 +/- 2 mV
4	Size*	nm (Diameter)	50 nm	50 +/- 15 nm

Table 1: A tabular organization of our design constraints and acceptable values, ranked by overall significance to the project.
*These metrics are sub-metrics of both the binding and transfection efficiency design metrics.

These design specifications were determined through a literature review, and discussions with our advisors, Dr. Richard Price and Anna Debski, as well as through prior experimentation. The zeta potential and size design specifications were discovered through discussions with Anna Debski as the novel nanoparticle being created is an optimization of a current nanoparticle used by her. These values have shown success with similar doses and in similar cell lines in the past. These values were also backed up by literature sources which showed that nanoparticles smaller than 200nm are ideal as any higher will activate the lymphatic system and become removed from circulation and that nanoparticles between 30 and 60 nm show the best binding ability [30], [31]. The values shown for zeta potential are verified by the literature which suggests that between -10 and 10 mV are best for binding [32]. The values for transfection efficiency and binding efficiency are based on past lipofectamine transfections. Transfections using lipofectamine done in the Price Lab by Anna Debski, Jackson Tirrell, and other lab members have generally seen around 20% transfection efficacy. We believe that these nanoparticles should show higher levels of transfection efficacy due to the expected higher levels of binding efficiency, which is caused by the more specific exofacial thiol targeting method, as opposed to lipofectamine's nonspecific binding and transfection, and the fact that PEI is considered the "gold standard" for plasmid transfections.

Materials and Methods

Cell Culture

All cells were maintained in a standard cell culture incubator at 37°C and 5% CO2. Mouse brain microvascular endothelial cells (bEnd.3) were cultured in DMEM supplemented with 10% fetal bovine serum and 1 mM sodium pyruvate. Murine glioma cells (GL261-Luc2) were cultured in DMEM supplemented with 10% fetal bovine serum, 1 mM nonessential amino acids, 1 mM sodium pyruvate, and 1mL geneticin. Cell flasks were cultured to 80% confluence on T-175 culture flasks and maintained at a low passage number.

Thiol Quantification

Performed using Ellman's reagent, 5,5'-Dithio-*bis*-(2-nitrobenzoic acid) $[C_{14}H_8N_2O_8S_2]$, a thiol-detecting chemical that forms a yellow colorimetric product upon reaction with free thiol groups [34]. Both cell lines were harvested from plates and counted, and 400,000 cells were resuspended in 500 uL of PBS. Ellman's reagent is then mixed with a reaction buffer (0.1M Na_3PO_4, pH 8.0, 1 mM EDTA) at a ratio of 2:100 [35]. This combined mixture was then added to each vial of cells and incubated for 15 minutes. The supernatant was then be isolated via centrifugation. Following this, spectrophotometric quantification of free thiols in the supernatant at 412 nm was performed.

Nanoparticle Formulation and Transfection

Nanoparticles are made using the PEI25K-g(20)-MPEG5K-SH polymer and PEI25K-g(20)-MPEG5K polymer from Nanosoft Biotechnology for the thiolated and unthiolated nanoparticles respectively. The PEG-PEI (Poly(ethylene glycol) - Polyethylenimine) polymer is combined with more PEI (To condense the nanoparticle size to allow for easier passage through the BBB), tris(2-chloroethyl) phosphate (TCEP, a reducing agent acting on existing disulfide bonds to preserve free thiols to allow for thiol-mediated binding). The unthiolated nanoparticle does not require the addition of TCEP. A GFP plasmid reporter was encapsulated by both the thiolated and unthiolated nanoparticles with the GFP signal representing transfection efficiency. An additional prep generated the same GFP plasmid labeled with a Cy5 fluorophore to assay binding. Nanoparticles are filtered prior to transfection with the thiolated group degassed with decafluorobutane to ensure disulfide bonds do not form. The completed nanoparticles are then transfected dropwise to the cells in an FBS-devoid media to minimize opsonization between the FBS proteins and the nanoparticles (0.5 ug/well of a 24-well plate) [36]. The cells were incubated with the nanoparticles for 4 hours before the media was aspirated and replaced with the complete media.

Thiol Concentration Modulation

In order to optimize the thiolation of the nanoparticles for targeting purposes, the nanoparticles were treated with varying concentrations of N-ethylmaleimide (NEM), which acts as a thiol-blocking agent by Falkylating thiol groups. The following concentrations of NEM 10x, 5x, 2x, 1x, 10^{-1}x, 10^{-2}x, 10^{-3}x, and 10^{-4}x were tested, relative to the concentrations of thiols in the polymer prior to nanoparticle formulation. Throughout the entire modulation protocol, the samples were degassed with decafluorobutane in order to prevent oxidation of the thiol groups via oxygen molecules in the air. Solid NEM was dissolved in Ultrapure H_2O at various concentrations, added to the thiolated polymer, and reacted at room temperature for two hours. After this incubation step, the samples were run through a desalting column to remove excess NEM from the solution that was not bound. To assay blocking levels, another Ellman's reagent assay was run, with lower absorbance values being indicative of the blocking of the thiol groups on the polymer.

In Vivo FUS Implementation

14 days post-inoculation, mice with Glioblastoma Multiforme (GBM) tumors will undergo FUS treatment. Firstly, these mice will be placed under ketamine and dexmedetomidine anesthesia and their heads will be shaved and an incision is made revealing the skull. The mice will be placed supine with degassed US gel on top of their heads and an ultrasound water basin placed on top of the gel. Tumors are treated using a 3-spot grid to cover the maximum area of the tumor. Optison microbubbles (MB) were administered at a concentration of $2*10^5$ MBs/g mouse weight. FUS treatments were performed using standard BBB opening procedures with a starting pressure of 0.2 MPa and a maximum pressure of 0.4 MPa and passive cavitation detection (PCD) monitoring.
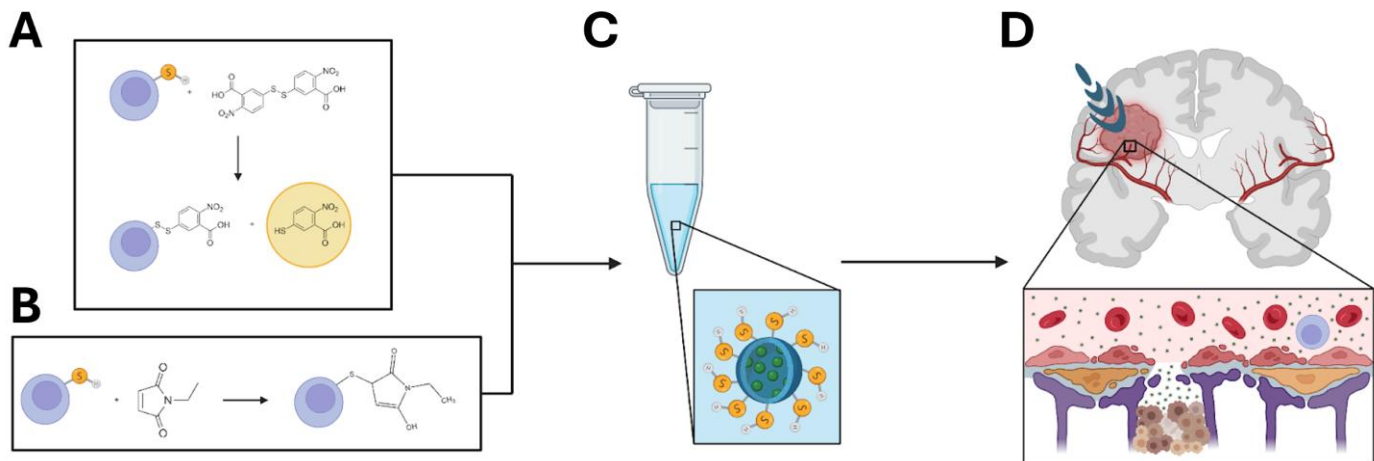
Figure 4: (A) Ellman's reagent was used to show that glioblastoma cancer cells have higher levels of accessible thiols compared to brain microvascular endothelial cells, identifying them as targets for thiolated nanoparticles, (B) N-ethylmaleimide used to modulate thiol concentration, (C) Thiolated PEG-PEI nanoparticles containing GFP reporter plasmids were synthesized to evaluate their binding and transfection efficiencies, (D) Focused ultrasound was used to open the blood-brain barrier in mice, allowing nanoparticles to reach glioblastoma sites. The delivery's success was monitored through flow cytometry of treated brain samples.

In order to optimize the timing of the FUS treatment, mice received an IV injection of nanoparticles loaded with 40μg plasmid DNA either 15 minutes before, at the start of, or 15 minutes after initiation of the FUS treatment. Two days following treatment, the mouse brain samples were harvested and prepared for flow cytometry.

Results & Discussion

Thiol Quantification
After the 400,00 bEnd.3 and Gl261-Luc2 cells were each resuspended and mixed with Ellman's reagent and the associated reaction buffer, and were analyzed using a spectrophotometer at a 412 nm wavelength for absorbance. Three samples for each cell type were assayed and absorbance values are visualized in Figure 5. The results indicated a significant increase in absorbance at 412 nm for the GL261-Luc2 cells when compared to the bEnd.3 cells via a t test ($p < 0.01$). The average reading for the GL261-Luc2 cells was 0.967, when compared to the bEnd.3 cells, which had an average value of 0.094 for absorbance, a decrease of over an order of magnitude. This validated prior literature claims that the GL261-Luc2 cells were more heavily thiolated than bEnd.3 cells in an *in vitro* setting, and therefore presented a potential intrinsic characteristic for targeting that can be leveraged for therapeutics.
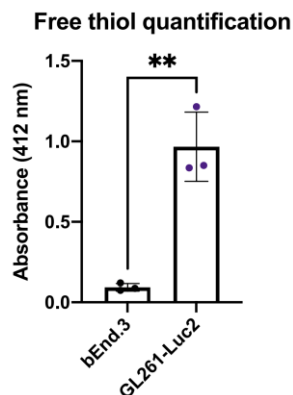

Figure 5: Free thiol levels in brain endothelial cell lines (bEnd.3) and in glioblastoma cell lines (GL261-Luc2) as quantified with Ellman's reagent. Significance found via T-test.

Nanoparticle Formulation and Transfection
The efficacy of our nanoparticle formulation protocol was evaluated through a zetasizer analysis of the finished nanoparticles in solution. On average, our synthesized nanoparticles were 61.09 nm in diameter and had a charge of -1.75 mV, both within the marginal bounds for success in our initial design constraints.

After the nanoparticles were formulated, they were transfected into GL261-Luc2 and bEnd.3 cells in a 24-well plate at a cell density of 30,000 cells/well. Both thiolated and unthiolated nanoparticles were used to transfect different cell triplicates and left to bind and transfect for 4 hours in FBS-free media to prevent interactions between the FBS and the thiol groups during nanoparticle delivery, after which the media was changed back to the standard GL261-Luc2 and bEnd.3 cell media. After this, the cells were sent for flow cytometry to assay both the binding efficiency by detecting the Cy5-labelled plasmid (binding efficiency) and GFP protein from the reporter plasmid (transfection efficiency) via nanoparticle delivery to the cells as seen in Figure 6.

Upon initial inspection, it seems that the thiolated nanoparticles in the GL261-Luc2 group did not perform as well as initially hypothesized, having a lower relative binding and transfection efficiency on average than many other conditions tested. However, Figure 7 shows the ratio of transfection efficiency to binding efficiency of each condition tested, and shows the much higher ratio of transfection into GL261-Luc2 cells by our thiolated nanoparticles compared to every other condition (bEnd.3 transfected with thiolated nanoparticles: 0.137, bEnd.3 cells transfected with unthiolated nanoparticles: 0.294, GL261-Luc2 cells transfected with thiolated nanoparticles: 0.521, GL251-Luc2 cells transfected with unthiolated nanoparticles: 0.266). In fact, the difference between the bEnd.3 (T) condition and the GL261-Luc2 (T) in their transfection:binding ratios has a significance value of $p = 0.0558$, implying marginal significance via an unpaired t-test. This demonstrates that our thiolated nanoparticles preferentially transfect into cancerous cells, and with more data sets than the triplicates we initially ran, the significance of this phenomenon might be proven.
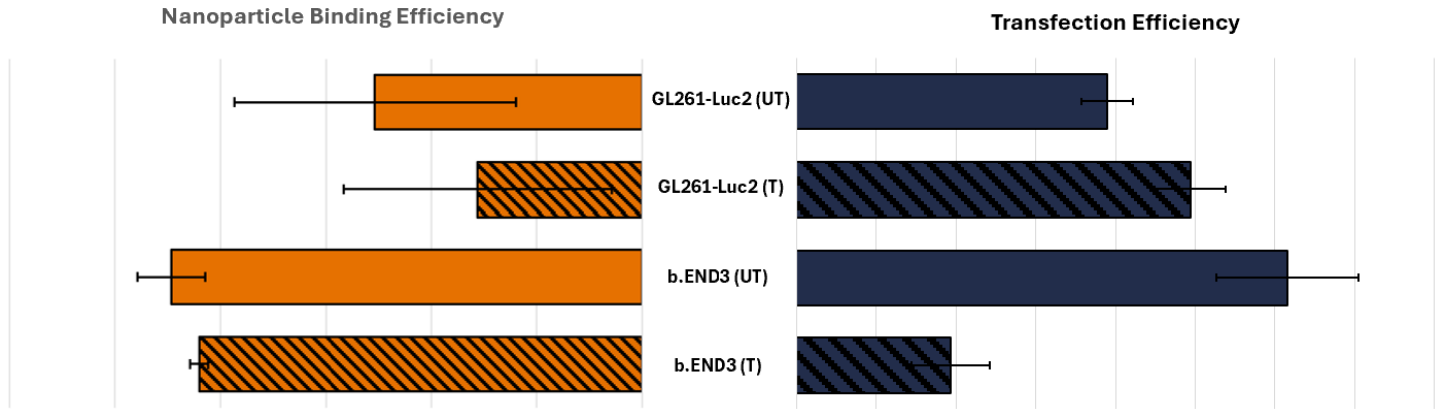
Nanoparticle Binding Efficiency | **Transfection Efficiency**

Figure 6: Synthesized thiolated (T) and unthiolated (UT) nanoparticle binding and transfection efficiencies measured using Cy5 (binding) and GFP (transfection) fluorescence.

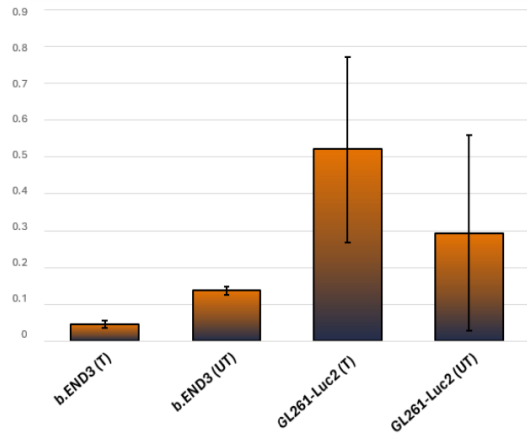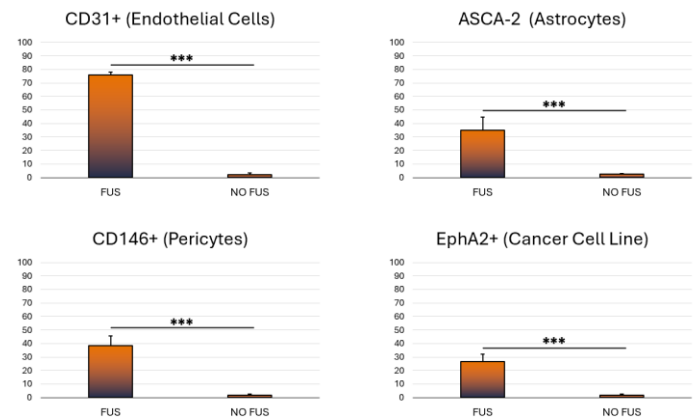**Transfection Efficiency : Binding Efficiency**

Figure 7: Synthesized thiolated (T) and unthiolated (UT) nanoparticle binding and transfection binding ratio (transfection / binding).

Thiol Concentration Modulation

Upon receiving the Ellman's reagent data for the 10x, 5x, 2x, 1x, 10^{-1}x, and 10^{-2}x concentrations of NEM, it was discovered that each and every one blocked all the thiols on the polymer. This was seen as the normal polymer absorbance value of 2.31, whereas the average for the NEM concentrated samples was 1.93. This difference in absorbance represents a difference in $\sim 3 \times 10^{-7}$ moles of thiol difference between the groups. The theoretical number of thiols on the nanoparticle is $\sim 1.9 \times 10^{-7}$ moles. These values imply that the blocking was complete, as the observed blocked thiol groups are higher in number than the ideal number of thiols. This data showed a need to pursue lower concentrations of NEM for effective and controlled blocking. Following this, a new experiment was performed that included 10^{-1}x, 10^{-2}x, 10^{-3}x, and 10^{-4}x groups. Due to errors with the TCEP blank that was used in the last experiment and intended to be used here, the unaltered polymer itself was used as a blank. Upon using this blank, absorbance values of 0.009, -0.018, -0.034, and 0.001 were found for the 10^{-1}x, 10^{-2}x, 10^{-3}x, and 10^{-4}x groups respectively. Given the nature of the blanking, a negative value implied blocked thiols, while a positive one did not. This data contradicted the previously obtained data by showing that the 10^{-1}x group did not block any thiols. Given the non-ideal blanking conditions, this data is less trustworthy than the previously mentioned set, and as such, this experiment should be repeated.

In Vivo FUS Implementation

After the mouse brain samples were harvested and sent for flow cytometry analysis, hierarchical gating of common neural cell markers was used in order to sort, identify, and quantify transfected cells. The four main markers of interest in the scope of this project were CD31+ (Endothelial Cells), ASCA-2 (Astrocytes), CD146+ (Pericytes), and EphA2+ (Glioblastoma cells). The different timeframes were investigated to determine the optimal manner for the FUS and thiolated nanoparticles to be implemented together. There was no significant difference in the transfection levels of cells between the 3 timepoints measured, but it seemed that overall FUS treatment 15 minutes before had the most optimal trends for transfection, with higher transfection % in the cancer cells, pericytes, and astrocytes (Supplementary Figures 1-4). This group had the lowest transfection into the endothelial cells, which is ideal as it implies more of the nanoparticle is passing the tight junctions and binding deeper in the brain. The finding that FUS treatment before nanoparticle injection shows the highest transfection in three groups of interest would support the hypothesis that FUS may interact with the disulfide bonds in a negative way but given the lack of significant data this claim cannot be made. The flow cytometry results between the delivery of the nanoparticles 15 minutes after FUS and the standard injection delivery of the nanoparticles is visualized in Figures 8-11, for each of the corresponding cell markers via absorbance units following the flow cytometry of the homogenized and prepped mouse brain samples. Across each condition, FUS treatment dramatically improved

Figures 8-11: *In Vivo* transfection efficiency of thiolated nanoparticles with and without aid from FUC-mediated BBB opening, evaluated by absorbance after flow cytometry.

transfection efficiency of the nanoparticle delivery compared to only doing nanoparticle injection ($p < 0.0001$). This demonstrates the efficacy and vitality of using FUS to mediate the delivery of our thiolated nanoparticles to our areas of interest within the brain, and with more time-point trials, an optimal FUS protocol can be elucidated for further delivery optimization.

Conclusions

This study has made progress in addressing the challenges of delivering therapeutic agents across the BBB to treat glioblastomas, leveraging the biochemical characteristics of the TME. The study began with verifying the increased presence of exofacial thiols in glioblastoma cell lines compared to normal brain endothelial cells, establishing the foundation for the rest of our study and assays. Subsequent analysis of our design for a PEG-PEI thiolated nanoparticles demonstrated that these nanoparticles preferentially transfected cancer cells when the binding efficiency parameter was normalized between the cell groups and thiolated vs. unthiolated nanoparticle conditions. The last critical finding of our study was done through the incorporation of FUS with microbubbles to disrupt the BBB. This method significantly enhanced the permeability of our thiolated nanoparticles into the brain's parenchyma. Our results showed that the combination of thiol-targeting nanoparticles and FUS treatment improved the delivery and transfection efficiencies in a glioblastoma model. Notably, the use of FUS enabled a more precise and controlled delivery of nanoparticles, which is crucial for reducing potential systemic side effects and increasing the therapeutic index of administered treatments.

This work was limited by its inability to accurately block thiol groups to produce a known concentration of these groups with NEM. While this work did show that the NEM can block these groups, additional work will need to be done to accurately block groups at specified percentage increments. The validation of increased free thiols in cancer cells relative to endothelial cells is significant but is limited by its *in vitro* setting as the whole of the TME is not involved. The finding that the ratio of transfection efficiency to binding efficiency is higher in cancer cells treated with the thiolated nanoparticles rather than the unthiolated nanoparticles or endothelial cells is an important finding but again does not yield a full picture due to its *in vitro* nature. While our *in vivo* study has promising results even this portion is limited due to the fact that an animal model is not a perfect representation of how the nanoparticle would interact in human tissue.

Future work for this study should look towards continuing attempts to modulate the number of thiol groups on the nanoparticle that can bind to our cells of interest. This experimentation will help determine the most optimal concentration of thiol groups and can determine the type of relationship present. Additional further study should look at the interaction between FUS and thiolated nanoparticles. The direct impact of FUS on disulfide bonds should be studied in an attempt to elucidate a deeper understanding of the timing of FUS treatment and its impact. This can be compounded by increasing the timeline of study for FUS application to 30 minutes before and after nanoparticle delivery to see if a larger difference is seen that maintains the pattern observed in the 15 minutes before and after the experiment. Finally, these nanoparticles should be tested in a variety of other tumor types to determine if increased transfection is seen relative to unthiolated nanoparticles and thus if the nanoparticle may have broader applications.

End Matter

References

[1] J. R. McFaline-Figueroa and E. Q. Lee, "Brain Tumors," Am. J. Med., vol. 131, no. 8, pp. 874–882, Aug. 2018, doi: 10.1016/j.amjmed.2017.12.039.

[2] Y. Takeshita and R. M. Ransohoff, "Inflammatory cell trafficking across the blood-brain barrier (BBB): Chemokine regulation and in vitro models," Immunol. Rev., vol. 248, no. 1, pp. 228–239, Jul. 2012, doi: 10.1111/j.1600-065X.2012.01127.x.

[3] C. Gasca-Salas et al., "Blood-brain barrier opening with focused ultrasound in Parkinson's disease dementia," Nat. Commun., vol. 12, no. 1, Art. no. 1, Feb. 2021, doi: 10.1038/s41467-021-21022-9.

[4] L. W. Xu, K. K. H. Chow, M. Lim, and G. Li, "Current Vaccine Trials in Glioblastoma: A Review," J. Immunol. Res., vol. 2014, p. 796856, 2014, doi: 10.1155/2014/796856.

[5] L. Ampie, E. C. Woolf, and C. Dardis, "Immunotherapeutic Advancements for Glioblastoma," Front. Oncol., vol. 5, p. 12, Jan. 2015, doi: 10.3389/fonc.2015.00012.

[6] K. Singh et al., "Enhancing T Cell Chemotaxis and Infiltration in Glioblastoma," Cancers, vol. 13, no. 21, p. 5367, Oct. 2021, doi: 10.3390/cancers13215367.

[7] F. Hanif, K. Muzaffar, K. Perveen, S. M. Malhi, and S. U. Simjee, "Glioblastoma Multiforme: A Review of its Epidemiology and Pathogenesis through Clinical Presentation and Treatment," Asian Pac. J. Cancer Prev. APJCP, vol. 18, no. 1, pp. 3–9, 2017, doi: 10.22034/APJCP.2017.18.1.3.

[8] M. V. Sofroniew and H. V. Vinters, "Astrocytes: biology and pathology," Acta Neuropathol. (Berl.), vol. 119, no. 1, pp. 7–35, 2010, doi: 10.1007/s00401-009-0619-8.

[9] M. Demeule, A. Régina, B. Annabi, Y. Bertrand, M. W. Bojanowski, and R. Béliveau, "Brain Endothelial Cells as Pharmacological Targets in Brain Tumors," Mol. Neurobiol., vol. 30, no. 2, pp. 157–184, 2004, doi: 10.1385/MN:30:2:157.

[10] R. P. Thomas, L. W. Xu, R. M. Lober, G. Li, and S. Nagpal, "The incidence and significance of multiple lesions in glioblastoma," J. Neurooncol., vol. 112, no. 1, pp. 91–97, Mar. 2013, doi: 10.1007/s11060-012-1030-1.

[11] S.-M. Razavi, K. E. Lee, B. E. Jin, P. S. Aujla, S. Gholamin, and G. Li, "Immune Evasion Strategies of Glioblastoma," Front. Surg., vol. 3, p. 11, Mar. 2016, doi: 10.3389/fsurg.2016.00011.

[12] S. Ray, M. M. Bonafede, and N. A. Mohile, "Treatment Patterns, Survival, and Healthcare Costs of Patients with Malignant Gliomas in a Large US Commercially Insured Population," Am. Health Drug Benefits, vol. 7, no. 3, pp. 140–149, May 2014.

[13] S. A. McIntosh et al., "Global funding for cancer research between 2016 and 2020: a content analysis of public and philanthropic investments," Lancet Oncol., vol. 24, no. 6, pp. 636–645, Jun. 2023, doi: 10.1016/S1470-2045(23)00182-1.

[14] C. M. Gorick et al., "Applications of focused ultrasound-mediated blood-brain barrier opening," Adv. Drug Deliv. Rev., vol. 191, p. 114583, Dec. 2022, doi: 10.1016/j.addr.2022.114583.

[15] Q. Ding et al., "CXCL9: evidence and contradictions for its role in tumor progression," Cancer Med., vol. 5, no. 11, pp. 3246–3259, 2016, doi: 10.1002/cam4.934.

[16] W. M. Pardridge, "The Blood-Brain Barrier: Bottleneck in Brain Drug Development," NeuroRX, vol. 2, no. 1, pp. 3–14, Jan. 2005, doi: 10.1602/neurorx.2.1.3.

[17] N. M. Anderson and M. C. Simon, "Tumor Microenvironment," Curr. Biol. CB, vol. 30, no. 16, pp. R921–R925, Aug. 2020, doi: 10.1016/j.cub.2020.06.081.

[18] X. Jiang et al., "The role of microenvironment in tumor angiogenesis," J. Exp. Clin. Cancer Res., vol. 39, no. 1, p. 204, Sep. 2020, doi: 10.1186/s13046-020-01709-5.

[19] "Tumor Microenvironment - an overview | ScienceDirect Topics." Accessed: Nov. 08, 2023. [Online]. Available: https://www.sciencedirect.com/topics/medicine-and-dentistry/tumor-microenvironment

[20] "Frontiers | The role of innate immune cells in the tumor microenvironment and research progress in anti-tumor therapy." Accessed: Nov. 08, 2023. [Online]. Available: https://www.frontiersin.org/articles/10.3389/fimmu.2022.1039260/full

[21] R. M. Linville et al., "A tissue-engineered model of the blood-tumor barrier during metastatic breast cancer," Fluids Barriers CNS, vol. 20, no. 1, p. 80, Nov. 2023, doi: 10.1186/s12987-023-00482-9.

[22] J. Pizzorno, "Glutathione!," Integr. Med. Clin. J., vol. 13, no. 1, pp. 8–12, Feb. 2014.

[23] "Glutathione - an overview | ScienceDirect Topics." Accessed: Nov. 08, 2023. [Online]. Available: https://www.sciencedirect.com/topics/medicine-and-dentistry/glutathione

[24] L. Kennedy, J. K. Sandhu, M.-E. Harper, and M. Cuperlovic-Culf, "Role of Glutathione in Cancer: From Mechanisms to Therapies," Biomolecules, vol. 10, no. 10, p. 1429, Oct. 2020, doi: 10.3390/biom10101429.

[25] A. Bansal and M. C. Simon, "Glutathione metabolism in cancer progression and treatment resistance," J. Cell Biol., vol. 217, no. 7, pp. 2291–2298, Jul. 2018, doi: 10.1083/jcb.201804161.

[26] H. Nsairat, D. Khater, U. Sayed, F. Odeh, A. A. Bawab, and W. Alshaer, "Liposomes: structure, composition, types, and clinical applications," Heliyon, vol. 8, no. 5, May 2022, doi: 10.1016/j.heliyon.2022.e09394.

[27] H. Lu, S. Zhang, J. Wang, and Q. Chen, "A Review on Polymer and Lipid-Based Nanocarriers and Its Application to Nano-Pharmaceutical and Food-Based Systems," Front. Nutr., vol. 8, p. 783831, Dec. 2021, doi: 10.3389/fnut.2021.783831.

[28] X.-Y. Lu, D.-C. Wu, Z.-J. Li, and G.-Q. Chen, "Chpater 7 - Polymer Nanoparticles," in Progress in Molecular Biology and Translational Science, vol. 104, A. Villaverde, Ed., in Nanoparticles in Translational Science and Medicine, vol. 104. , Academic Press, 2011, pp. 299–323. doi: 10.1016/B978-0-12-416020-0.00007-3.

[29] "Polymer Nanoparticles - an overview | ScienceDirect Topics." Accessed: Nov. 08, 2023. [Online]. Available: https://www.sciencedirect.com/topics/materials-science/polymer-nanoparticles#:~:text=Polymeric%20nanoparticles%20are%20organic%2Dbased,and%20receptor%2Dmediated%20drug%20delivery.

[30] A. J. Slezak et al., "Tumor Cell-Surface Binding of Immune Stimulating Polymeric Glyco-Adjuvant via Cysteine-Reactive Pyridyl Disulfide Promotes Antitumor Immunity," ACS Cent. Sci., vol. 8, no. 10, pp. 1435–1446, Oct. 2022, doi: 10.1021/acscentsci.2c00704.

[31] S. A. A. Rizvi and A. M. Saleh, "Applications of nanoparticle systems in drug delivery technology," Saudi Pharm. J. SPJ, vol. 26, no. 1, pp. 64–70, Jan. 2018, doi: 10.1016/j.jsps.2017.10.012.

[32] N. Hoshyar, S. Gray, H. Han, and G. Bao, "The effect of nanoparticle size on in vivo pharmacokinetics and cellular interaction," Nanomed., vol. 11, no. 6, pp. 673–692, Mar. 2016, doi: 10.2217/nnm.16.5.

[33] J. D. Clogston and A. K. Patri, "Zeta potential measurement," Methods Mol. Biol. Clifton NJ, vol. 697, pp. 63–70, 2011, doi: 10.1007/978-1-60327-198-1_6.

[34] "DTNB (Ellman's Reagent) (5,5-dithio-bis-(2-nitrobenzoic acid))." Accessed: Oct. 24, 2023. [Online]. Available: https://www.thermofisher.com/order/catalog/product/22582

[35] "Elman's Reagent Protocol." Accessed: Nov. 09, 2023. [Online]. Available: https://www.thermofisher.com/document-connect/document-connect.html?url=https://assets.thermofisher.com/TFS-Assets%2FLSG%2Fmanuals%2FMAN0011216_Ellmans_Reag_UG.pdf

[36] T. U. Wani, S. N. Raza, and N. A. Khan, "Nanoparticle opsonization: forces involved and protection by long chain polymers," Polym. Bull., vol. 77, no. 7, pp. 3865–3889, Jul. 2020, doi: 10.1007/s00289-019-02924-7.

Supplementary Figures
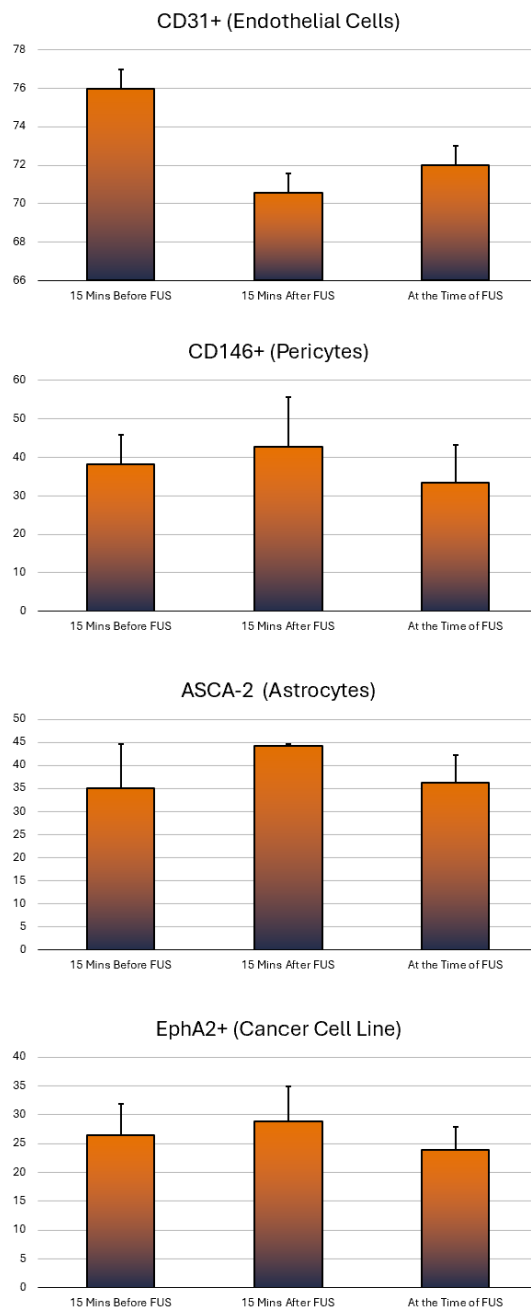
Supplementary Figures 1-4: Absorbance values of brain samples with variable nanoparticle injection times relative to FUS administration.